

PROCESSING AND CHARACTERISATION OF HIGH-VELOCITY SUSPENSION FLAME SPRAYED (HVSFS) BIOACTIVE GLASS COATINGS

GIOVANNI BOLELLI, VALERIA CANNILLO, RAINER GADOW*,
ANDREAS KILLINGER*, LUCA LUSVARGHI, JOHANNES RAUCH*

*Department of Materials and Environmental Engineering, University of Modena and Reggio Emilia,
Via Vignolese 905, I-41100 Modena, Italy*

**Institute for Manufacturing Technologies of Ceramic Components and Composites (IMTCCC), University of Stuttgart,
Allmandring 7b, D-70569 Stuttgart, Germany*

E-mail: giovanni.bolelli@unimore.it

Submitted December 8, 2009; accepted February 9, 2010

Keywords: High-Velocity Suspension Flame Spraying (HVSFS), Bioactive glass coatings, Suspension rheology, Scanning electron microscopy (SEM), Micro-Raman spectroscopy

The High-Velocity Suspension Flame Spraying (HVSFS) technique was employed in order to deposit bioactive glass coatings onto titanium substrates. Two different glass compositions were examined: the classical 45S5 Bioglass and a newly-developed $\text{SiO}_2\text{-CaO-K}_2\text{O-P}_2\text{O}_5$ glass, labelled as "Bio-K". Suitable raw materials were melted in a furnace and fritted by casting into water. The frit was dry-milled in a porcelain jar and subsequently attrition-milled in isopropanol. The resulting micron-sized powders were dispersed in a water+isopropanol mixture, in order to prepare suitable suspensions for the HVSFS process. The deposition parameters were varied; however, all coatings were obtained by performing three consecutive torch cycles in front of the substrate. The thickness and porosity of the coatings were significantly affected by the chosen set of deposition parameters; however, in all cases, the layer produced during the third torch cycle was thicker and denser than the one produced during the first cycle. As the system temperature increases during the spraying process, the particles sprayed during the last torch cycle remain at $T > T_g$ while they spread, so that interlamellar viscous flow sintering takes place, favouring the formation of such denser microstructure. Both coatings are entirely glassy; however, micro-Raman spectroscopy reveals that, whereas the 45S5 coating is structurally identical to the corresponding bulk glass, the "Bio-K" coating is somewhat different from the bulk one.

INTRODUCTION

Thermal spraying of bio-active glasses offers the opportunity to coat titanium implants with tailored layers for different medical applications. The resorption of the coating can be adjusted by its chemical composition and microstructure as a monovariant of the processing. Additionally, thermally-sprayed bioglasses do not generally undergo as large chemical and structural alterations as hydroxyapatite does [1,2].

Conventional thermal spray techniques, like APS or HVOF, however, were shown to produce highly defective glass coatings, requiring post-deposition heat treatments [3,4].

The novel HVSFS technique gives the possibility to process glass frits and produce dense, well adherent coatings on titanium substrates [5]. The basic concept of the HVSFS process is given elsewhere [6].

MANUFACTURING TECHNOLOGY

Preparation of powders and suspensions

Two different bio-active glasses were employed in these experiments: the classical 45S5 Bioglass, with chemical composition (in weight %) 45.0 % SiO_2 , 6.0 % P_2O_5 , 24.5 % CaO , 24.5 % Na_2O [7], and a newly-developed bioglass, designated as "Bio-K" and consisting of 39.8 % SiO_2 , 21.8 % CaO , 33.1 % K_2O , 5.3 % P_2O_5 (in weight %). Reagent-grade raw materials were mixed in stoichiometric amounts and melted in a Pt crucible kept at 1650 °C for 1 h, using an electrical furnace; frits were then obtained by casting the molten glasses into water and were dry-milled in porcelain jars using 10 mm-diameter Al_2O_3 balls. The resulting powders, sieved below 45 μm , were subsequently attrition milled in isopropanol for 3 h using 5 mm-diameter ZrO_2 balls and dried.

Suspensions were produced by dispersing 20 wt.% of attrition-milled powder in 80 wt.% of a liquid phase consisting of 60 wt.% water + 40 wt.% isopropanol. A de-flocculating agent (Dolapix-65, 0.5 wt.%) was also added to the suspension.

Rheological properties of the suspensions

To ensure a stable process, the suspensions must possess low viscosity and fine particle size ($<10 \mu\text{m}$). The particle shape should be spherical.

The rheological properties of the used bio-glass suspensions were determined by rotating mode on a Physica rheometer device. 100.0 ml of suspension were tested in an aluminium beaker with a cylindrical rotating measurement device.

Both suspensions show a shear thinning behaviour (Figure 1): at low shear stress, the viscosity of the Bio-K suspension has a value of $\sim 0.9 \text{ Pa}\cdot\text{s}$ and that of the Bioglass suspension is $\sim 0.2 \text{ Pa}\cdot\text{s}$; at a shear rate of 100 s^{-1} , the viscosity decreases in both cases to about $0.01 \text{ Pa}\cdot\text{s}$.

Particle size distribution

The particle size distribution of the two attrition-milled glass powders was measured with a laser granulometer (Mastersizer, Malvern). The Bio-K powder had a grain size distribution of $D_{10} = 0.86 \mu\text{m}$, $D_{50} = 1.99 \mu\text{m}$ and $D_{90} = 5.01 \mu\text{m}$, while the 45S5 powder had a size distribution of $D_{10} = 1.13 \mu\text{m}$, $D_{50} = 4.69 \mu\text{m}$ and $D_{90} = 14.12 \mu\text{m}$, as shown in Figure 2.

The SEM images show that the shape of the 45S5 Bioglass is blocky after attrition milling with few particles larger than $10 \mu\text{m}$. The shape of the Bio-K glass particles is much finer with particles smaller than $5 \mu\text{m}$ (Figure 3).

Pretreatment of the substrates

Titanium grade 2 plates ($50 \times 50 \text{ mm}^2$) were cleaned with acetone before grit blasting with FEPA 120 fine corundum with 5 bar pressure. The surface roughness after grit blasting process was $R_a = 1.49 \mu\text{m}$ and $R_z = 9.99 \mu\text{m}$.

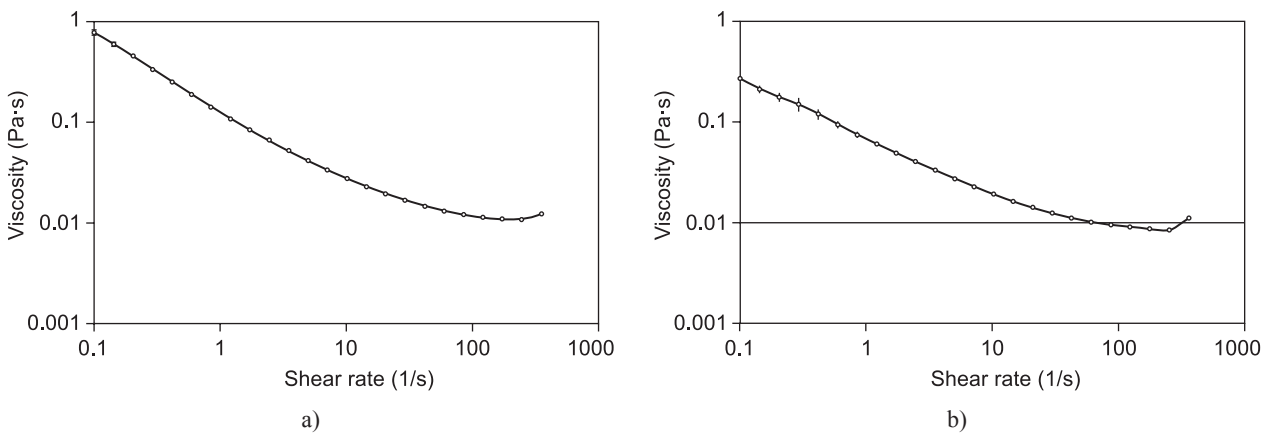


Figure 1. Viscosity curves of the Bio-K suspension (a) and of the 45S5 Bioglass suspension (b).

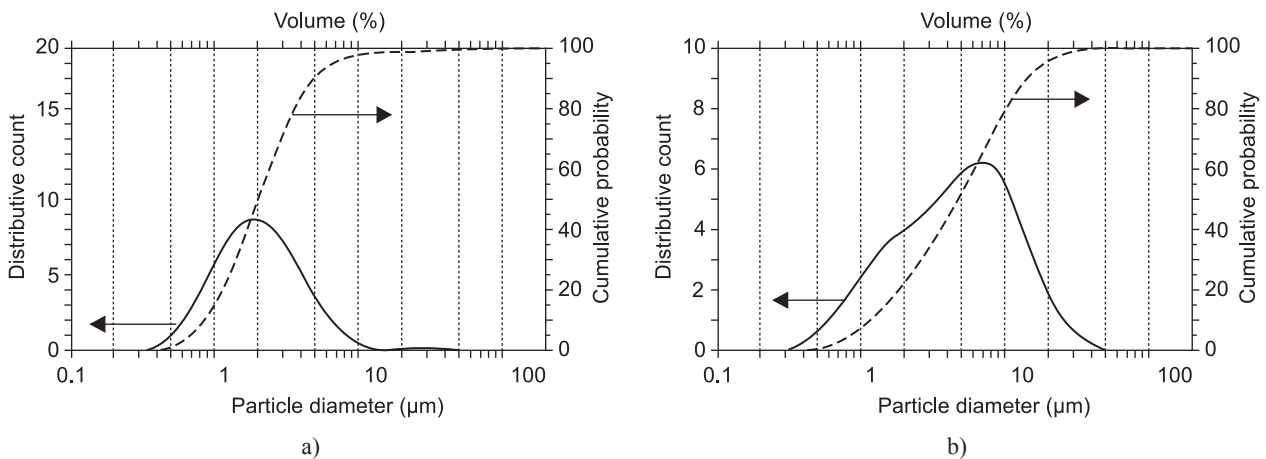


Figure 2. Particle size distribution of the Bio-K (a) and 45S5 Bioglass (b) powders after attrition milling.

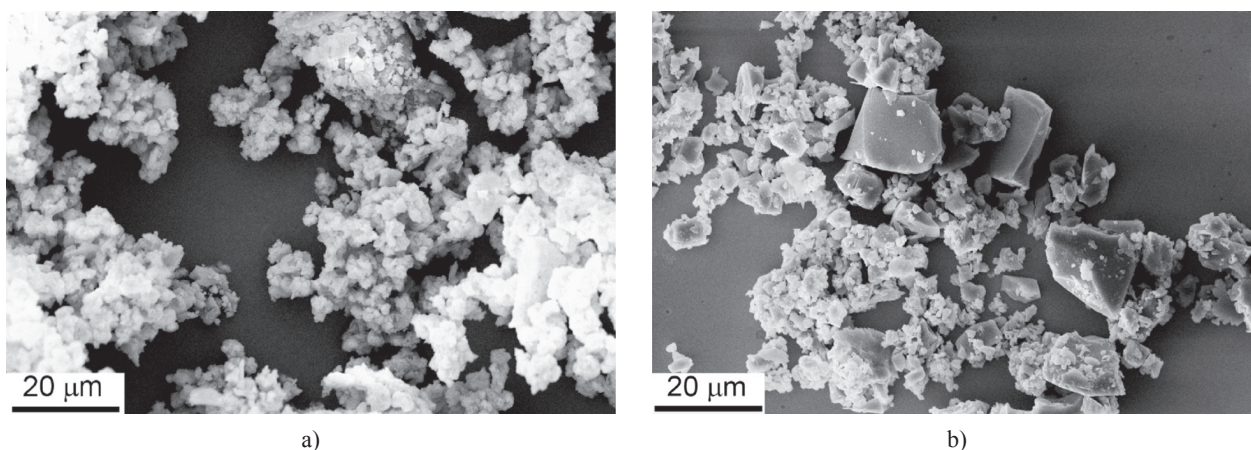


Figure 3. SEM images of the glass powders after attrition milling. A: Bio-K, B: 45S5 Bioglass.

Coating experiments

Five different coatings were deposited using the 45S5 Bioglass powder: the suspension feed rate, the fuel (propane) and oxygen flow rates and the stand-off distance were varied (Table 1). The HVSFS torch was mounted on a six axis robot; each coating was deposited by performing 3 torch cycles, each consisting of a meander trajectory with 600 mm/s pass velocity and 2 mm inter-pass distance.

The substrates were always pre-heated to about 100 °C with one torch cycle, before coating deposition. The temperature was controlled by a pyrometer (Keller, Germany) focused on the front side of the samples.

At the present stage of the research, a lower number of experiments have been performed on the Bio-K glass: only two deposition parameter sets have been tested up to now (Table 1).

COATING PROPERTIES

45S5 Bioglass coatings

In the 45S5 Bioglass coatings, the three layers deposited during the three torch cycles (see section

Coating experiments) can be easily recognized, as they are separated by clear porosity lines (see dash-dot lines on polished cross-sections, Figure 4a-e, and arrows on fractured section views, Figure 5a). Very remarkably, the layer thickness and porosity vary at each torch cycle, i.e. the first (bottom) layer is thin and exhibits abundant fine porosity, whereas the third (topmost) layer becomes significantly (3 times or more) thicker, with few large spherical pores. This morphological alteration is particularly obvious when the pump speed (i.e., the suspension feed rate) was maximum (Figures 4b,c).

The large, rounded pores in the top layer are definitely similar to those which can be produced during viscous flow sintering of a conventional glaze, as a result of air entrainment [8]. The inter-layer porosity, by contrast, seems to be caused by the presence of hollow rounded particles (see fractured sections on Figures 5a,b): pores are contributed both by the intra-particle cavities and by the inter-particles voids, on account of their incomplete flattening. Analogously, these hollow rounded particles also seem to produce the fine and homogeneously-distributed pores of the first layer (Figures 4,5).

The following coating formation mechanism can be proposed. When the suspension flow is injected into the torch gas jet, it is fragmented into small droplets and the solvent subsequently evaporates [9].

Table 1. Deposition parameters for the 45S5 Bioglass and the Bio-K coatings.

Sample ID	O ₂ flow rate (Sl/min)	Propane flow rate (Sl/min)	Stand-off distance (mm)	Pump speed (% of maximum)/ /resulting volume flow rate (cm ³ /s)
Bioglass 1	325	45	100	60 % / 2.5
Bioglass 2	350	45	100	70 % / 3.3
Bioglass 3	325	45	100	70 % / 3.3
Bioglass 4	325	45	100	65 % / 2.9
Bioglass 5	350	55	120	70 % / 3.3
Bio-K 1	300	45	120	65 % / 2.9
Bio-K 2	265	45	120	65 % / 2.9

While some of the largest particles could be released at this stage as individual particles, in most cases (and especially when the finer, sub-micrometric particles are involved) agglomeration occurs [9]. The shear-thinning behaviour of the suspension also suggests the particles tend to flocculate and form large agglomerates, which are progressively disrupted as the shear rate increases. As the suspension injector has an internal diameter of 1.2 mm and it is about 20 mm long, an approximate estimation suggests that a fully-developed laminar flow

($Re \sim 50$) can be established before reaching the injector exit. The shear rate therefore varies along the injector's cross-section, from a minimum (zero) along its axis, to a maximum of $\sim 2 \times 10^5 \text{ s}^{-1}$ close to its wall. Consequently, a wide agglomerate size distribution, encompassing both large non-disrupted agglomerates and fine ones (resulting from disruption due to large shear rates close to the walls), is injected into the combustion chamber. Additionally, as the solvent evaporation during suspension thermal spraying is very fast ($\sim 1 \mu\text{s}$), the

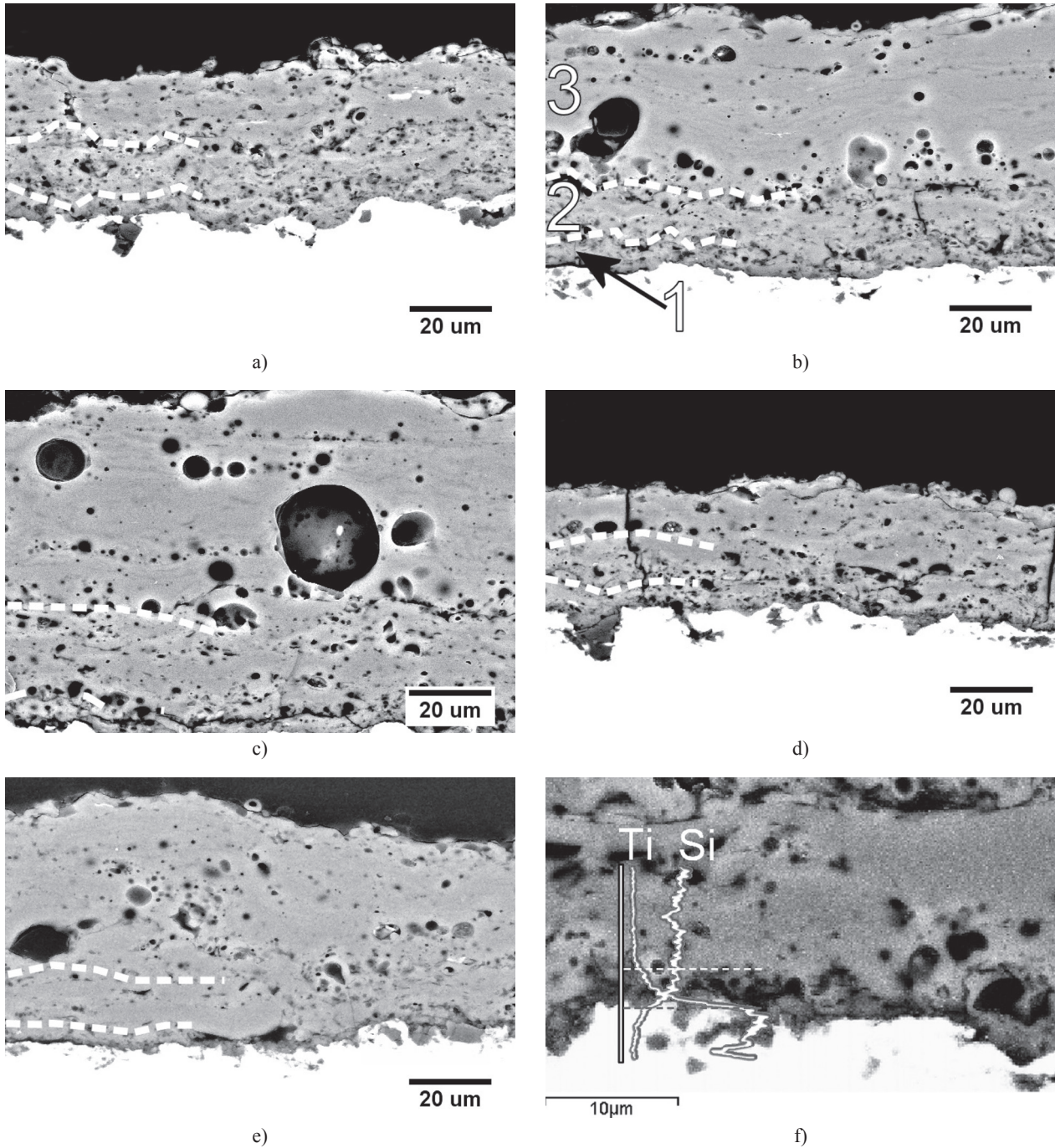


Figure 4. Cross-sectional SEM micrographs (backscattered electrons) of the Bioglass-1 (a), 2 (b), 3 (c), 4 (d), 5 (e) coatings (dash-dot lines mark the boundaries between the three coating layers) and EDX line-scan analysis along the coating-substrate interface of Bioglass-4 sample (f).

agglomerates (especially the smaller ones) may take a hollow morphology, as it occurs in a spray-drying process when the solvent evaporates very rapidly from a droplet [10].

Most likely, during the spraying process, the larger agglomerates cannot be fully melted, because of the low thermal conductivity of glass. The smaller ones ($\sim 1 \mu\text{m}$), formed by the finest (sub-micrometric) particles (see the particle size distribution in Figure 2b), by contrast, have such low inertia [11] that they probably start slowing and cooling down before impacting onto the substrate, so that the impact probably occurs at a temperature which is just slightly above the glass transition temperature (T_g). Some of the small agglomerates could even be ejected away from the gas jet axis and into the colder jet fringes because of the low inertia, as shown in [12].

As a consequence, when depositing the first coating layer onto a moderately pre-heated substrate (the pre-heating temperature of about 100°C is well below the glass transition temperature), most of the large agglomerates rebound (because they are mainly unmelted), thus impairing the deposition efficiency. The smaller agglomerates can be deposited, but their low kinetic energy (caused both by low impact velocity and by the low density of the glass, about 2.4 g/cm^3 [13]) and their low impact temperature (coupled to the relatively low substrate temperature) cause them to cool below T_g before they can spread significantly. The first coating layer is therefore thin and contains non-flattened particles retaining their original hollow morphology.

The particles caught in the jet fringes are less heated than those in the jet core, so that the retention of the hollow rounded morphology is enhanced, and travel slower, so that they impinge onto the target with a certain delay. These particles are therefore deposited on top of each coating layer and produce the previously-described interlayer porosity.

After each torch cycle, the sample surface temperature (continuously monitored by the Keller pyrometer)

increases: the third layer is therefore deposited on top of a much warmer, pre-deposited glass layer. When heated glass particles impinge onto such warm glass layer, they do not cool as fast as onto the metal substrate; therefore, they remain above T_g long enough to spread and adhere to the underlying material [13,14]; additionally, upon particle impact, the surrounding glass could also be reheated above T_g . Consequently, larger agglomerates can stick to the surrounding material and be embedded in the coating, even when they are not completely melted (see Figure 4e), improving the deposition efficiency. Moreover, the small hollow particles have the time to flow and flatten, so that the overall porosity decreases. During the third cycle, in particular, the surface temperature becomes so large that the particles remain above T_g during their whole spreading process, so that viscous flow sintering between the lamellae takes place [14].

The deposition efficiency enhancement becomes particularly remarkable when the suspension feed rate is larger (samples Bioglass-2 and Bioglass-3): during the first cycle, only a very small fraction of the impinging material is deposited, whereas, during the third one, a much larger fraction contributes to the layer formation. The deposition of a large amount of material which remains above T_g during the entire spreading process may result in the coalescence of very large gas bubbles, giving rise to large spherical pores [14]. These pores are not removed from the coating, both because the available time was too short and because, during the present experiments, the samples were kept in a vertical position, which means the gas bubbles would tend to move parallel to the substrate, rather than towards the top surface. In some of the samples, large tensile stresses were probably developed because of the extremely large amount of material deposited during the third pass, leading to the formation of transverse cracks (Figure 4d).

It should also be noted that a thin titanium oxide film (recognisable as a thin dark layer in the cross-sectional

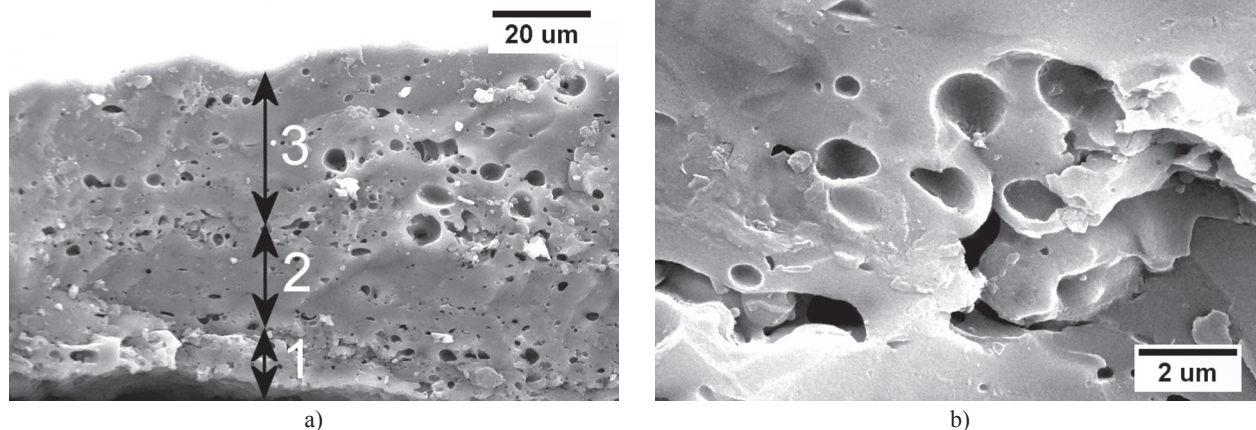


Figure 5. Overview (a) and detail (b) of the fractured surface (secondary electron-SEM micrographs) of the Bioglass-2 coating. The arrows in panel (a) mark the three coating layers.

micrographs of Figure 4) is formed on top of the substrate, as a consequence of pre-heating and of the increasingly large sample temperature during coating deposition. The EDX line-scan analyses (Figure 4f) confirm the formation of a Ti oxide-based layer. The Si-K α peak also remains quite intense while scanning through this thin layer (Figure 4f, see the region delimited by dashed lines); however, due to the quite poor lateral resolution of the EDX technique (the EDX signal generation region is ≥ 1 μm large), it is presently not possible to clarify whether some chemical interaction could occur between the glass coating and the Ti oxide layer. In any case, this layer is of the utmost importance for coating adhesion; indeed, it was experimentally observed that a continuous, adherent glass coating could never be formed without pre-heating, irrespective of the chosen deposition parameters.

XRD analysis reveals that the coatings retained a fully glassy structure; additionally, micro-Raman spectroscopy does not indicate any structural alteration in the HVSFS-deposited 45S5 Bioglass layers, as compared to its bulk (cast and annealed) equivalent (Figure 6a).

Bio-K coatings

Optimisation is still needed for the Bio-K coatings; indeed, the two coatings deposited so far (particularly sample Bio-K 2) are quite thin and possess remarkable porosity (Figure 7). As the glass transition temperature of the Bio-K glass ($T_g = 520$ $^{\circ}\text{C}$, from DTA analysis) is slightly lower than that of the 45S5 Bioglass ($T_g = 550$ $^{\circ}\text{C}$ [15]), it was indeed chosen to employ parameters which would generate lower flame temperatures and would keep the sample surface colder, in order to avoid excessive overheating of the deposited layer, which might have brought to the formation of excessively large gas bubbles and excessively large tensile stresses. It is, however, quite clear that the presently-selected deposition conditions generated too low deposition temperatures. The impinging droplets were cooled below T_g before spreading was complete, so that many small agglomerates retained their hollow, rounded morphology and no large agglomerate was embedded.

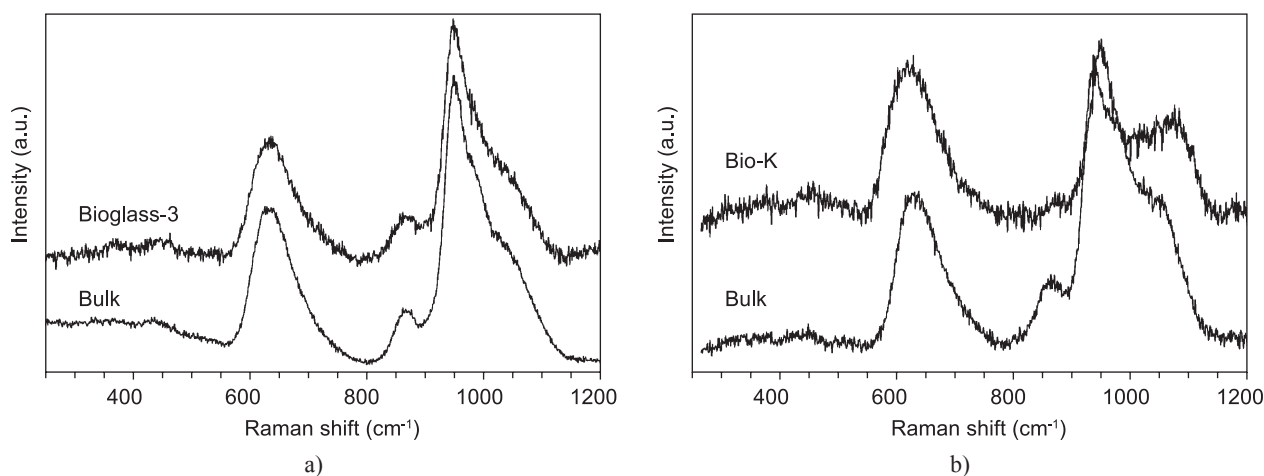


Figure 6. Raman spectra of the Bioglass-3 (a) and Bio-K 1 (b) samples, compared to the spectra of the correspondent bulk glasses.

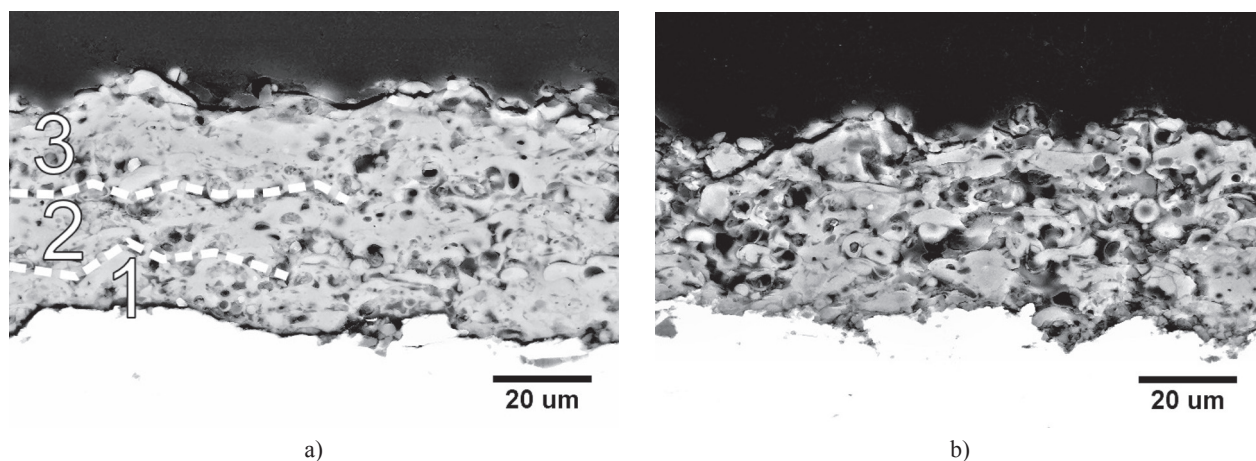


Figure 7. Cross-sectional SEM micrographs (backscattered electrons) of the Bio-K1 (a) and Bio-K 2 (b) coatings. The dash-dot lines mark the boundaries between the three coating layers.

The Bio-K coatings are completely glassy (as revealed by XRD); however, the Raman spectra acquired on the two Bio-K coatings differ significantly from the spectrum of the bulk Bio-K glass (Figure 6b). Fitting the 800-1 280 cm^{-1} region with gaussian peak functions reveals that the bulk Bio-K glass exhibits peaks at 862 cm^{-1} , 933 cm^{-1} , 965 cm^{-1} and 1 052 cm^{-1} . According to ref. [16], these peaks can be assigned to the symmetric stretching of SiO_4^{4-} monomers, symmetric stretching of $\text{Si}_2\text{O}_6^{4-}$ chain and ring structures, stretching of the P–O–P network and asymmetric stretching of the SiO_2 three-dimensional network, respectively. In the HVSFS-deposited coatings, peaks are located at 869 cm^{-1} , 948 cm^{-1} , 1 000 cm^{-1} and 1 081 cm^{-1} : the first two peaks, although somewhat shifted, can still be assigned to the symmetric stretching of SiO_4^{4-} monomers and of $\text{Si}_2\text{O}_6^{4-}$ chain and ring structures (respectively). The third peak now belongs to the $^0\text{O–P–O}$ stretching in P_2O_5 sheet units and the fourth belongs to $\text{Si}_2\text{O}_5^{2-}$ planar structures [16]: in the coatings, the peaks belonging to the three-dimensional silica and phosphor networks therefore became so weak that they cannot be recognized any more, and were replaced by peaks belonging to planar structures ($\text{Si}_2\text{O}_5^{2-}$ units and P_2O_5 sheets). This is a clear indication of a degradation of the three-dimensional glass network in the HVSFS-deposited Bio-K coating.

CONCLUSIONS

These results suggest the HVSFS technique is a viable technique for the production of high-quality bioactive glass coatings onto Ti substrates. Careful control over the processing parameters is required; specifically, the surface temperature of the sample during spraying critically affects the deposition efficiency and the microstructure of each coating layer. In order to achieve high deposition efficiency and dense layers, the system must be warm enough, so that the impinging particles are allowed to remain above T_g during spreading, but excessive overheating would lead to the formation of very large pores and to stress accumulation. Further work should therefore aim to optimize the deposition of the Bio-K glass and to devise strategies to

improve the deposition efficiency during the first torch cycle; for instance, a possibility would be to deposit a ceramic bond coat (e.g. TiO_2) and to pre-heat the system to larger temperatures before HVSFS bioglass spraying. Moreover, the reasons for the structural alteration of the Bio-K glass after spraying must be investigated.

References

1. Dyshlovenko S., Pawlowski L., Pateyron B., Smurov I., Harding J.H.: *Surf.Coat.Technol.* 200, 3757 (2006).
2. Sun L., Berndt C.C., Gross K.A., Kucuk A.: *J.Biomed. Mater.Res.* 58, 570 (2001).
3. Cannillo V., Pierli F., Sampath S., Siligardi C.: *J.Eur.Ceram. Soc.* 27, 4575 (2007).
4. Bolelli G., Lusvardi L., Manfredini T., Parsini E., Siligardi C.: *J.Eur.Ceram.Soc.* 27, 4575 (2007).
5. Bolelli G., Cannillo V., Gadow R., Killinger A., Lusvardi L., Rauch J.: *J.Eur.Ceram.Soc.* 29, 2249 (2009).
6. Killinger A., Kuhn M., Gadow R.: *Surf.Coat.Technol.* 201, 1922 (2006).
7. Hench L. L.: *J.Am.Ceram.Soc.* 81, 1705 (1998).
8. Bolelli G., Cannillo V., Lusvardi L., Manfredini T., Siligardi C., Bartuli C., Loreto A., Valente T.: *J.Eur.Ceram. Soc.* 25, 1835 (2005).
9. Delbos C., Fazilleau J., Rat V., Coudert J. F., Fauchais P., Pateyron B.: *PlasmaChem.PlasmaProcess.* 26, 393 (2006).
10. Kaßner H., Vaßen R., Stöver D.: *Surf.Coat.Technol.* 202, 4355 (2008).
11. Dongmo E., Wenzelburger M., Gadow R.: *Surf.Coat.Technol.* 202, 4470 (2008).
12. Srivatsan V. R., Dolatabadi A.: *J.Therm.SprayTechnol.* 15, 481 (2006).
13. Poirier T., Planche M.P., Landemarre O., Coddet C.: *J. Therm.SprayTechnol.* 17, 564 (2008).
14. Arcondéguy A., Grimaud A., Denoirjean A., Gasgnier G., Hugué C., Pateyron B., Montavon G., *J.Therm. Spray Technol.* 16, 978 (2007).
15. Lefebvre L., Chevalier J., Gremillard L., Zenati R., Thollet G., Bernache-Assolant D., Govin A.: *ActaMater.* 55, 3305 (2007).
16. Lin C.-C., Huang L.-C., Shen P.: *J.Non-Cryst.Solids* 351, 3195 (2005).